Lattice Matched Tunable Wavelength GeSn Quantum Well Laser Architecture: Theoretical Investigation

Rutwik Joshi, Luke F. Lester, *Fellow*, IEEE, and Mantu K. Hudait, *Senior Member, IEEE*

Abstract— In this work, we propose an initial framework and present numerical estimates for designing a GeSn-based quantum well (QW) laser that can attain efficient lasing, while utilizing a monolithic lattice matched (LM) InGaAs/GeSn/InGaAs stack. GeSn QW emission characteristics depend significantly on the quantized energy level as the bulk bandgap reduces and approaches zero for high Sn. One factor that diminishes the quantum efficiency of light sources is the defects within the active region, which result in non-radiative recombination. Furthermore, defects at the interface can hinder the band alignment causing loss of carrier confinement. InGaAs, InAlAs and a well-designed LGB can provide large band offsets with GeSn to form a type I separate confinement heterostructure (SCH) QW laser structure while enabling a virtually defect-free active region suitable for room temperature operation and scalable to an arbitrary number of QWs. When LM, the InAlAs and InGaAs layers provide a large total band offset of ~1.1eV and ~0.6eV, respectively. For a 10 nm GeSn QW SCH laser, a threshold current (J_{TH}) of ~ 10 A/cm^2 can be achieved at an emission wavelength of ~ 2.6 μm with a net material and modal gain of ~ 3000 cm^{-1} and ~ 40 cm^{-1}, respectively. The J_{TH} and net gain can be optimized for the InAlAs/InGaAs/GeSn/InGaAs/InAlAs SCH laser structure for Sn between 8-18% by adaptively designing the SCH waveguide and QW. Through adaptive waveguide design, quantization, and Sn alloying, a wide application space (1.2μm to 6μm) can be covered.

Index Terms— Quantum well laser, GeSn, InGaAs/InAlAs, monolithic light source, Lattice matched GeSn laser, tensile GeSn.

I. INTRODUCTION

Growing interest in germanium (Ge) and GeSn-based optoelectronic devices for applications beyond silicon (Si) transistors [1-3], optical components, detectors, and light sources [4-7] makes a Ge-based monolithic photonic platform an interesting exploration. The recent rise in integrated quantum technologies can be accelerated if the diverse quantum components utilizing potentially incompatible materials systems can be co-integrated heterogeneously using a chiplet-based approach [8]. This heterogeneous integration can be potentially simplified if the materials are Si-compatible or directly integrable on Si. Consequently, many reports over the last two decades have made tremendous progress in integrating Ge [9, 10], GeSn, and SiGeSn [11, 12] materials on Si to form optoelectronic devices.

The growth of GeSn directly on Si suffers from a large lattice mismatch, which causes defects and dislocations in the GeSn active layer [10], which can be inferred through the minority carrier lifetime [13]. Achieving a high carrier lifetime in the GeSn (or Ge) epitaxial layer is a key challenge in realizing efficient light sources [14] since defects become sites of non-radiative recombination. Interestingly, the GaAs material system ($In_xGa_{1-x}As$ and $In_xAl_{1-x}As$) due to its lattice proximity to $Ge_{1-y}Sn_y$ can provide lattice matched or low-strain quantum well (QW) barriers and waveguide layers for a GeSn laser structure. Furthermore, the InAlAs/InGaAs/GeSn/InGaAs/InAlAs separate confinement heterostructure (SCH) QW structure is transferrable to a Si substrate *via* a graded buffer formed either with $In_xGa_{1-x}As$ or $In_xAl_{1-x}As$ [4,13].

Implementing Ge-based light sources on Si is expected to be more challenging than conventional commercial III-V lasers, due to several key challenges: (i) growth of device quality defect-free Ge or GeSn, (ii) sufficient band offsets to form type I carrier confinement, (iii) refractive index step or gradient for optical confinement, and (iv) in-direct bandgap nature of Ge and large density of states (DOS) in the L-valley. Although integrating GeSn on Si directly using Si/GeSn heterostructure may provide extensive advantages such as (i) manufacturability ease due to Si compatibility, (ii) use of simple Si-based binary and/or ternary alloys, and (iii) cost-benefit, it is challenging to provide the key attributes required for efficient room temperature lasing. However, the growth of GeSn on Si poses certain hurdles due to (i) increased lattice mismatch, (ii) low carrier lifetime due to lattice relaxation-induced defects, and (iii) low band offsets between the active and barrier layers. Historically, to achieve all the key attributes required for efficient room temperature lasing, commercial direct-gap III-V compound semiconductor-based lasers have employed
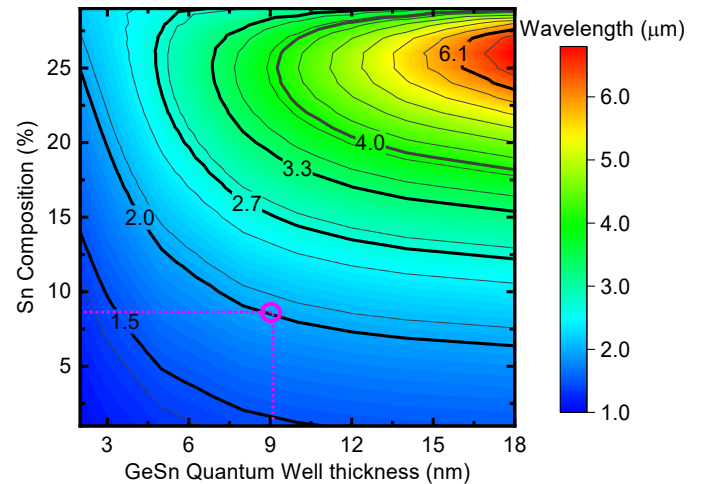
Fig. 1. Large tunability (1.2 μm to 6 μm wavelength) of the proposed GeSn/InGaAs/InAlAs SCH QW laser structure as a function of the Sn composition in GeSn QW and the QW thickness. A sample design point is marked for lasing operation at a wavelength of 2 μm considering the HH-band to Γ-valley ground state sub-band transition.
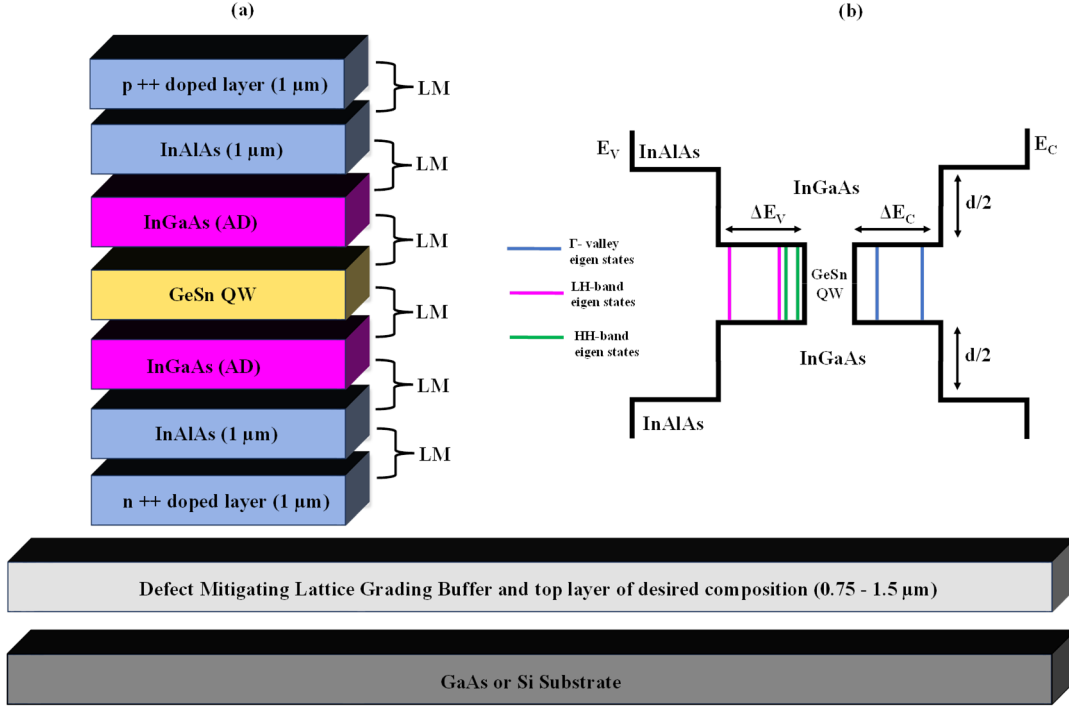
Fig. 2. GeSn QW laser and SCH waveguide structure which utilizes a lattice matched stack (*i.e.*, each of the heterointerfaces is LM) grown on a GaAs or Si substrate. The LM GeSn laser waveguide simulation structure (a) GeSn/InGaAs/InAlAs SCH QW grown on a GaAs substrate and transferrable to Si and (b) the corresponding schematic band structure associated with the SCH QW. The acronym AD is shown for the InGaAs waveguide layers to indicate that the thickness is chosen according to the adaptive design methodology to adapt and optimize the optical confinement factor to the changing emission characteristics.

complex layer stacks involving different compositions of ternary, quaternary, and penta-atomic layers [15-17]. We expect that similarly designed III-V layer stacks serving the purpose of lattice matching, lattice grading, lattice straining, refractive index grading, carrier confinement, and waveguide will be required for achieving lasing from the GeSn active layer.

In this work, we propose and analyze the use of $In_xGa_{1-x}As$ and $In_xAl_{1-x}As$ compositionally controlled epitaxial layers to form a SCH QW structure for the GeSn active layer. The key merit of this design is that the complete QW laser stack (GeSn QW, InGaAs waveguide, and barrier, InAlAs SCH layer, and contact layers) can be lattice matched, resulting in no lattice-mismatched induced defects and potentially superior as well as reliable lasing performance. Additionally, the $In_xGa_{1-x}As$ and $In_xAl_{1-x}As$ layers can provide large band offsets with the GeSn layer to form a type I system with operability at room temperature. Furthermore, the lack of defects at the interfaces can mitigate any defect-induced band alignment changes [18] away from type I. The impact of Sn composition and the GeSn QW thickness on the key laser metrics such as bandgap energies, offsets, wavelength of emission, optical confinement factor, and waveguide design, are evaluated. The methodology of lattice matching $In_xGa_{1-x}As$ and $In_xAl_{1-x}As$ layers to compositionally controlled GeSn is examined to highlight the importance of tunability and design ease. Using TCAD solvers with material properties calibrated to Ge and InGaAs [2,6], the 3D laser stack is evaluated using self-consistent numerical solvers to determine the potentials, currents, charge densities, fermi-levels, *etc* [6]. A custom gain solver is used to compute the QW laser performance metrics such as gain and J_{TH} [6]. The proposed InAlAs/InGaAs/GeSn/InGaAs/InAlAs SCH laser structure can achieve an excellent J_{TH} approaching ~ 10 A/cm^2 at an emission wavelength of ~ 2.6 µm while providing good

net modal gain for a single QW configuration of ~ 40 cm^{-1}. As a consequence of Sn composition-dependent lasing wavelength, effective mass, bandgap, and conductivity of the stack, the proposed GeSn laser can perform optimally for Sn compositions between 8 - 18 %. Consequential implications of the GeSn/InGaAs QW system such as low joint-DOS, low effective mass, Γ- and L-valley energies and separation, quantum confinement, composition dependence, polarization dependence, and their impact on the lasing performance are discussed. Lastly, a lattice-mismatched modification to the GeSn/InGaAs QW laser structure is proposed that deviates marginally and controllably from the lattice matched case. This controlled lattice mismatch can be engineered using the InAs composition in the waveguide. As the avenue of GeSn light sources evolves certain applications may demand a small degree of compressive or tensile strain in the GeSn active layer, similar to GeSn on SiGeSn system with added potential advantages. Furthermore, it may be challenging to obtain a perfect lattice matched (or even a perfectly controlled strain) system in the real world although linearly graded buffer (LGB) has been studied extensively over the years. Hence, the possibility of controlling the In composition in graded InGaAs buffer can enable a "knob" to tune the lasing performance, offset the lattice mismatch or attain mismatch intentionally to enable appropriate lasing performance.

This LM GeSn QW SCH laser has the potential to be an efficient, reliable, and tunable (1.2 µm to 6 µm wavelength) room-temperature light source, which can be monolithically integrated on a GaAs or Si substrate. The wide range of tunability of this GeSn QW laser as a function of Sn alloy composition and GeSn QW thickness is shown in **Fig. 1**. Using the 30×30 **k.p** calculations for GeSn, the DOS effective mass and band energy trends are used in calculating the first few sub-
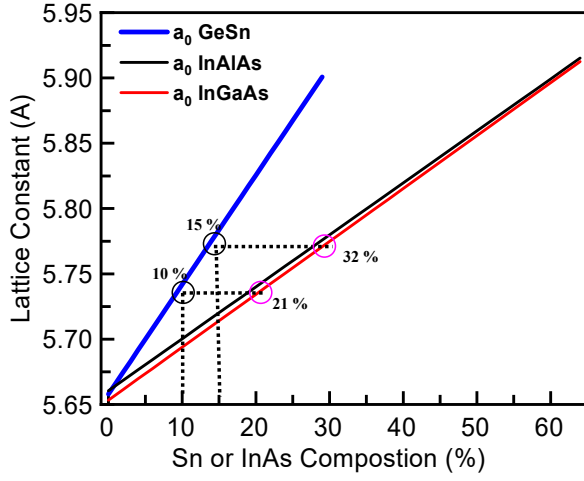
Fig. 3. The lattice constants of the 3 materials, GeSn, InGaAs and InAlAs which form the proposed lattice matched GeSn QW SCH laser as a function of their alloy compositions. For a given Sn composition in GeSn, by approximately doubling the InAs composition in the InGaAs (or InAlAs) waveguide layer or barrier layer, one can achieve lattice matching.

band energies in the Γ-valley, LH-band, and HH-band. The InGaAs QW barrier height and thickness are determined through the adaptive waveguide design discussed below and in turn used to find the eigen energies in this finite QW system. Each transition according to Fermi's golden rule is evaluated, obtaining higher transition strength for the HH-band transitions owing to the larger DOS of the HH-band. The emission wavelength in **Fig. 1** is the difference in the sub-band energies for the HH-band to Γ-valley transition in the GeSn QW. Similar wavelength peaks (compared with Fig. 1) have been observed in various studies over the years for GeSn, as part of theoretical and experimental studies: emission at ~ 2.2 µm for Sn 11 % [12], ~ 2.7 µm at Sn = 13 % [12] and ~ 2.8 µm at Sn = 16 % [19]. The other possible emission peaks are discussed in later sections. Particular wavelength contours for important applications are highlighted such as optical communication at 1.5 µm and extended-spectrum for fiber communication at 2 µm [20], gas sensing C-H stretch at 3.3 µm [21], and missile defense. The proposed system can have a wide range of applications such as daytime quantum key distribution (QKD) [22], integrated Si optics and quantum sensing [23, 24], and probing of gas molecules [25].

II. MATERIAL GROWTH AND STRUCTURES

A schematic representation of the proposed GeSn QW laser structure is shown in **Fig. 2**, which also represents the sample structure used for simulations and predictions in this work. The structure can be grown on a GaAs or Si substrate *via* a lattice grading $In_xGa_{1-x}As$ or $In_xAl_{1-x}As$ buffer to translate the lattice constant to the desired Sn composition in GeSn QW while mitigating the defects and dislocations in the active layer. The LGB design and implementation are crucial for the proposed laser structure as the LGB is expected to contain a dense network of misfit defects while attaining the desired InAlAs or InGaAs composition from the GaAs substrate. Once the desired composition in the LGB is reached, the layer is topped off with a thick layer of the desired composition InGaAs or InAlAs to ensure that the lasing active region is further away from the LGB defects and is truly relaxed. For systems where the LGB

did not relax completely resulting in small residual strains such as 0.1 %, the critical layer thicknesses are very large approaching the micrometer range, exponentially. Here, the strain relaxation-induced defects are a very small concern. We have demonstrated such fully relaxed InGaAs/InAlAs LGB in the past for many compositions of InGaAs and InAlAs buffers [4, 10, 13, 26], the methodology to do so has been well studied over the years. The structure will then involve *p*- and *n*-type doped regions outside the SCH structure, which provide the carriers for injection into the GeSn QW. This growth of GeSn QW structures is realized through vacuum interconnected dual chamber solid source molecular beam epitaxy (MBE) [13, 26]. The proposed design shown in **Fig. 2 (a)** involves GeSn sandwiched between two LM $In_xGa_{1-x}As$ layers to form the GeSn QW laser structure. The $In_xAl_{1-x}As$ layers form the SCH for confining the optical field thus enhancing the optical confinement factor through a large refractive index step. This structure utilizes a GeSn-on-$In_xGa_{1-x}As$ heterointerface which is expected to provide good band offsets for carrier confinement. The direct MBE growth of GeSn on $In_xGa_{1-x}As$ is preferred over $In_xAl_{1-x}As$ (although both are LM to GeSn) due to the higher surface roughness of InAlAs than InGaAs where the ad-atom surface mobility of aluminum is lower than gallium [27]. Since the $In_xAl_{1-x}As$/$In_xGa_{1-x}As$/GeSn/$In_xGa_{1-x}As$/$In_xAl_{1-x}As$ SCH QW structure is LM, the constraint of the critical layer thickness [18] is eliminated resulting in better design flexibility, reliability, fewer defects, higher carrier lifetime, and reduced free carrier absorption. Furthermore, limiting the relaxation-induced defects far away from the SCH lasing structure and within the LGB will benefit device performance regarding internal quantum efficiency (IQE) and band alignment [6, 14]. Eliminating the critical layer thickness limit for this laser stack also opens avenues for exploring multiple QW (MQW) structures based on GeSn. **Fig. 2 (b)** shows the schematic representation of the band structure of the $In_xAl_{1-x}As$/$In_xGa_{1-x}As$/GeSn/$In_xGa_{1-x}As$/$In_xAl_{1-x}As$ SCH QW structure. The various design metrics under consideration in this work are denoted in Fig. 2 (b) such as, (i) band offsets ΔE_C and ΔE_V, (ii) waveguide thickness d/2, and (iii) the electron and hole eigenstates in the CB and VB. The waveguide thickness d/2 is dependent on the Sn and In composition, corresponding refractive indices, and emission wavelength, and is chosen through an adaptive design methodology to optimize the optical confinement factor [6].

III. IMPORTANCE OF LATTICE MATCHING IN THE SCH

Sn alloying [11, 13, 25] and epitaxial tensile strain [4, 6, 9] are two techniques used to transition Ge to a direct bandgap material and make it an efficient light source. Both these techniques have certain challenges and drawbacks. For example, GeSn alloys pose processing/fabrication challenges as well as Sn clustering and segregation issues. Whereas the tensile Ge system has a certain critical layer thickness beyond which the strain field relaxes completely and creates defects and dislocations. In GeSn, the Sn alloying effect lowers the Γ-valley making GeSn a more direct bandgap active layer, but the presence of any compressive strain pushes the Γ-valley upwards resulting in a partial negation of the benefits of Sn alloying, *i.e.*, masking of the Sn-alloying beneficial effect. Interestingly, it is predicted that GeSn on Ge heteroepitaxial growths may never
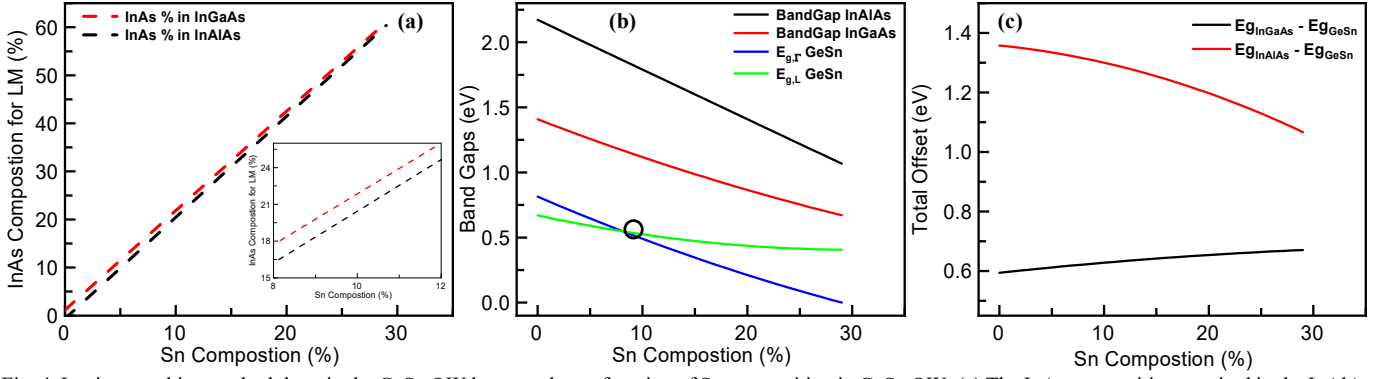
Fig. 4. Lattice matching methodology in the GeSn QW laser stack as a function of Sn composition in GeSn QW: (a) The InAs composition required in the InAlAs barrier layer and InGaAs waveguide layer to achieve lattice matching, and (b) the corresponding bandgaps of the 3 materials in the lattice matched SCH QW stack. (c) the total available band offset for the $Ge_{1-y}Sn_y$ LM SCH QW laser stack.

transition to a direct bandgap nature for any composition of Sn due to the compressive strain [28], and a similar trend can be expected for GeSn on GaAs or AlAs.

Lattice matching of the $Ge_{1-y}Sn_y$ QW with the SCH structure has certain benefits such as: (i) no critical layer thickness limit on GeSn layers creating ease for an arbitrary number of QWs, (ii) no strain field and strain relaxation induced defects, (iii) absence of compressive strain in GeSn avoids masking of Sn effect while preserving the energy separation between the Γ- and L-valley, (iv) better material quality and interfaces indicated through a high minority carrier lifetime, (v) higher band offsets and refractive index step, and (vi) improved IQE due to reduced non-radiative recombination. The radiative carrier recombination takes place in the GeSn active layer and the LGB defects are nearly 3 μm away from the GeSn layer, *see* Fig. 2. Also, there is a large refractive index step between the InGaAs and the InAlAs SCH (Δn ~ 0.3), sufficient to confine a large fraction of the electric field within the waveguide, with negligible amount reaching to the LGB. The impact of the LGB defects on the optical field and emission is thus assumed to be ignorable in this simulation framework, due to the LGB growth relaxation know-how and distance from the active region. Recently, $Ge_{0.94}Sn_{0.06}$ samples were grown using the MBE system on a lattice matched $In_{0.12}Al_{0.88}As$ underlayer [26]. Due to the lattice matched interface, the minority carrier lifetime measured through the microwave photoconductive decay (μ-PCD) technique was as high as 300 ns, indicating a good material quality and a drastically reduced Shockley–Read–Hall recombination, which would result in improved IQE [6, 14].

The adaptive methodology for lattice matching and composition choice of the waveguide and cladding layers formed by $In_xGa_{1-x}As$ and $In_xAl_{1-x}As$ is summarized in **Fig. 3**. *For example*, choosing Sn composition of 10 % in $Ge_{1-y}Sn_y$, one must set the InAs mole-fraction in $In_xGa_{1-x}As$ (the QW barrier and waveguide) and $In_xAl_{1-x}As$ (the SCH cladding) layers in the laser stack at nearly 21 %. Note that the composition is slightly different for $In_xGa_{1-x}As$ and $In_xAl_{1-x}As$ due to the small difference in lattice constants. In essence, the InAs composition in $In_xGa_{1-x}As$ and $In_xAl_{1-x}As$ must be about double that of the Sn composition in $Ge_{1-y}Sn_y$. The choice of Sn composition will depend on many aspects such as the wavelength of emission, IQE, gain, J_{TH}, gain, application requirement, *etc*., and the InAs composition will be set correspondingly based on the Sn composition, shown in **Fig. 4 (a)**. Once lattice matched to the choice of Sn composition in $Ge_{1-y}Sn_y$, the bandgaps of the 3 LM

materials $Ge_{1-y}Sn_y$, $In_xGa_{1-x}As$, and $In_xAl_{1-x}As$ are now dependent on the Sn composition as shown in **Fig. 4 (b)**. The transition point where $Ge_{1-y}Sn_y$ transitions to a direct bandgap material is visible as the intersection of the L-and Γ-valley energies at ~ 8% Sn. The SCH structure (*see* **Fig. 2a**) was chosen for the $Ge_{1-y}Sn_y$ QW as it provides good optical confinement through a refractive index step. It can be seen through **Fig. 4 (b)** that the bandgaps of $Ge_{1-y}Sn_y$, $In_xGa_{1-x}As$, and $In_xAl_{1-x}As$ were in increasing order of energy when all three layers were lattice matched for all Sn compositions. This implies that the refractive index would be in the decreasing order thus creating the required SCH step profile for confining the optical field within the waveguide, with InAlAs having the lowest refractive index. Although the exact band alignment of the $Ge_{1-y}Sn_y/In_xGa_{1-x}As$ interface as well as its composition dependence is not known, the total available band offset for this virtually defect-free interface can be estimated as shown in **Fig. 4 (c)**. The total band offset is the difference in the bandgaps of $Ge_{1-y}Sn_y$ and $In_xGa_{1-x}As$ or $In_xAl_{1-x}As$ at the corresponding LM composition. It is evident that at all Sn compositions, the proposed $Ge_{1-y}Sn_y$ SCH QW laser structure can provide large band offsets and a step profile of bandgaps suitable for SCH.

IV. RESULTS AND DISCUSSIONS

The emission characteristics of the proposed $Ge_{1-y}Sn_y$ SCH QW structure can be estimated through knowledge of the band properties. Through 30×30 **k.p** calculations [29], the band energies, effective masses, and composition dependence of various conduction bands (CBs) and valence bands (VBs) in $Ge_{1-y}Sn_y$ alloys are predicted [29]. The refractive index and band energies for $In_xGa_{1-x}As$ and $In_xAl_{1-x}As$ are adopted from Ref. 30. The 3-slab waveguide model was used to calculate the optical confinement in the $Ge_{1-y}Sn_y$ QW. The gain spectrum and threshold characteristics for the GeSn QW are calculated using a custom in-house gain solver [6, 15, 16] fed with 3D electrical profiles calculated through calibrated models via Sentaurus TCAD [31]. The simulation model includes the structure shown in Fig. 2 (a). This includes the barriers around the GeSn QW formed by InGaAs, and InAlAs cladding layers confining the
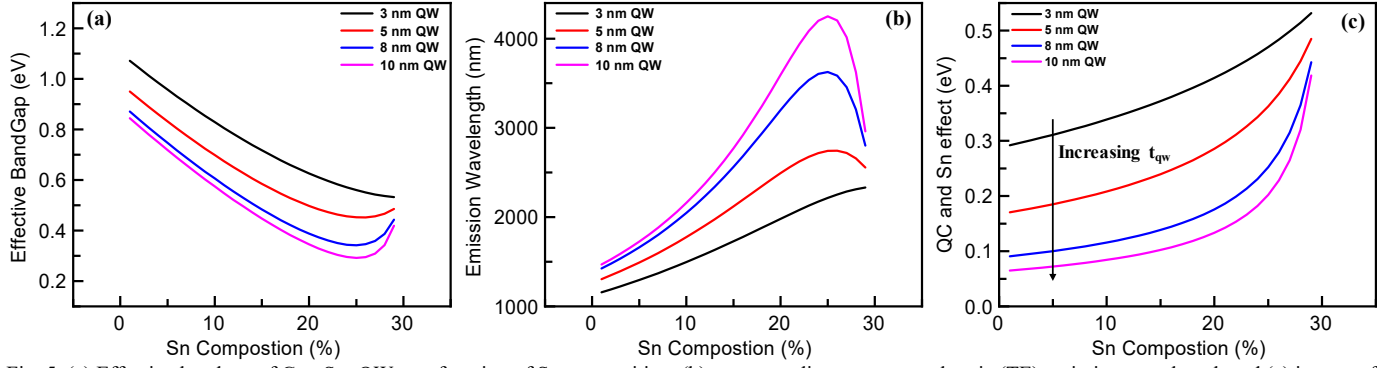
Fig. 5. (a) Effective bandgap of Ge$_{1-y}$Sn$_y$ QW as a function of Sn composition, (b) corresponding transverse electric (TE) emission wavelength and (c) impact of Sn alloying and quantization on the effective band edge as a function of Sn composition.

optical E-field through a large refractive index difference. Critical material properties are considered for each material utilizing a dense numerical meshing in the model. There is added confidence in the electrical profiles in the system as the material properties used for all III-V materials and Ge are physically detailed and well-calibrated by Synopsys Sentaurus TCAD [31] over the years and for Ge and InGaAs nanoscale-electrical device simulations [2, 3]. These models include a vast range of ideal and non-ideal physical phenomena such as multivalley band structure, MLDA, drift-diffusion, density gradient, various mole fractions, mobility and doping dependencies, *etc*. The electrical probes/contact are connected to the outermost layers, *i.e.*, the highly doped *n* and *p* regions so that electrical injection can spread into the entire laser stack, similar to where one would connect probes on a physically fabricated laser device. Along with the impact of the GeSn active region material properties, the results shown here include a large impact on the composition, mobility, band structure, thickness, conductivity, hetero-transport, refractive index, and doping of the III-V layers in the laser stack.

A. Effective band edge and emission wavelength of GeSn QW

As the Ge$_{1-y}$Sn$_y$ SCH QW is formed, the ground state eigen energies move to higher values, and the effective bandgap of the Ge$_{1-y}$Sn$_y$ QW is now larger than the bulk bandgap of Ge$_{1-y}$Sn$_y$. The impact of QW thickness on the quantization of energy levels and consequently the effective bandgap is shown in **Fig. 5 (a)** as a function of Sn composition in the Ge$_{1-y}$Sn$_y$ QW. The corresponding emission wavelength as a function of Sn composition in the Ge$_{1-y}$Sn$_y$ QW is shown in **Fig. 5 (b)**. Alloying with Sn produces a drastic reduction in the effective mass of the Γ-valley electrons in the CB as well as the LH-band which impacts the emission wavelength as seen in **Fig. 5 (b)**. The impact of Ge$_{1-y}$Sn$_y$ composition-dependent quantization can be understood through **Fig. 5 (c)**, which shows the impact on the effective bandgap beyond the bulk Ge$_{1-y}$Sn$_y$ bandgap. It is important to note that the emission from the Ge$_{1-y}$Sn$_y$ QW occurs largely from the Γ – HH transition resulting in transverse electric (TE) dominant emission [6, 32]. Emissions involving the LH-band, although nearly degenerate with the HH-band would have a smaller gain as the DOS of the LH-band is low [6]. Radiative emissions from the L-valley are unlikely and negligible compared to the transitions from the Γ-valley, but the impact of the large L-valley DOS on the carrier densities is significant here while affecting the J$_{TH}$ [6, 33].

B. Band offsets between Ge$_{1-y}$Sn$_y$/In$_x$Ga$_{1-x}$As

To estimate the valence band offset (VBO) and conduction band offset (CBO), certain assumptions need to be made regarding the VBO since no experimental results for compositional dependence of the Ge$_{1-y}$Sn$_y$/In$_x$Ga$_{1-x}$As band alignment are available. X-ray photoelectron spectroscopy measurement of Ge/GaAs structure was reported in Ref. 34 previously to determine the VBO and consequently the CBO. This VBO for the Ge/GaAs (*i.e.*, the Ge$_{1-y}$Sn$_y$/ In$_x$Ga$_{1-x}$As QW system for Sn = 0 %) has been determined to be nearly 0.35×ΔE$_g$, consequently, this is used as an assumption to determine the offsets for the Ge$_{1-y}$Sn$_y$/ In$_x$Ga$_{1-x}$As QW system as the compositions are changed. Note that the total offset is also summarized in **Fig. 4 (c)**. Based on these estimates, it is possible to determine if the carriers in the CB and VB will be confined in the QW even at room temperature. Note that due to the finite band offsets for the GeSn QW, the eigen energies as well as the electron and hole wavefunctions are calculated considering their offset dependence. The ground state eigen energies in the Γ-valley and the CBO are shown in **Fig 6 (a)** and the electrons in the Γ-valley would be confined for most of the Sn compositions. Similarly, the holes in the VB are confined in the HH-band, and the corresponding ground state eigen energies and band offset available are shown in **Fig. 6 (b)**. At higher Sn compositions due to the rising quantum confinement effect (QC) associated with the reduced effective mass of GeSn, the carriers are more likely to escape. Carrier confinement for the holes in the HH-band is not affected by the Sn alloying effect as the effective mass of the HH-band holes is large and doesn't change significantly, unlike the electrons in the Γ-valley and holes in the LH-band.

C. Adaptive waveguide design

One critical problem in the design of this tunable wavelength GeSn laser is that the waveguide needs to adapt to the emission wavelength dynamically to optimize the optical confinement factor and reduce the material losses. Hence, we utilize an adaptive design methodology previously discussed in detail in Ref. 6 to arrive at the thickness and composition numbers for the structure shown in Fig 2(a). The waveguide structure (thickness, composition) needs to be adapted to optimize the optical confinement ensuring a larger overlap of the QW with the E-field. For operation at 2.8 μm, the Sn composition must be ~ 15 %, consequently, the InGaAs (and InAlAs) composition to be ~ 30 %. Now that the compositions, bandgaps, and
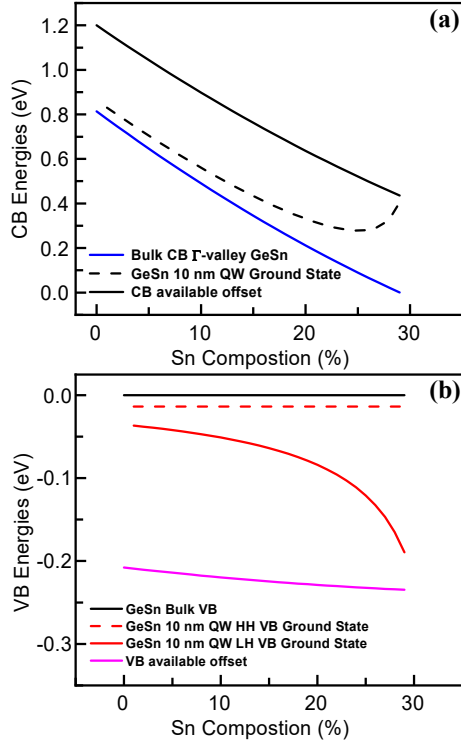
Fig. 6. Band-offsets and ground state eigen energies as a function of Sn composition for (a) the CB and (b) VB in the 10 nm GeSn QW with a LM InGaAs QW barrier.

refractive indices of the waveguiding layers are known, the choice of InGaAs thickness is crucial and is discussed including the adaptive design in **Fig. 7 (a)**. For a choice of Sn ~ 15 %, the waveguide thickness of InGaAs on each side must be ~ 350nm/2 *i.e.*, 175 nm. The optical confinement factor has an inflection point at this chosen value, and choosing a waveguide thickness above or below this would provide a drastically lower confinement factor [6]. Now if one chooses a Sn composition and chooses the right waveguide thickness based on the adaptive design, the best confinement factor can be obtained. This optimal confinement factor obtainable through adaptive design is shown in **Fig. 7 (b)**. Although the structure will house

propagation will be quasi-TE or quasi-TM with a mix of many modes, for simplification, we use the TE and TM acronyms.

D. Waveguide design and optical confinement factor

The emitted optical field confined in the 3-slab waveguide, the Sn composition in the $Ge_{1-y}Sn_y$ QW as well as the QW thickness will affect the confinement factor [6]. As the Sn composition in the $Ge_{1-y}Sn_y$ QW is increased, the emission wavelength increases while also affecting the refractive indices of the layers in the SCH waveguide. At longer wavelengths, confining the optical field within the waveguide (*i.e.*, with a large optical confinement factor) becomes challenging. This is because, the refractive index of the InGaAs waveguiding layers confining the wave reduces, resulting in a smaller SCH refractive index step (Δn) between the waveguide and the SCH cladding, and consequently poorer optical confinement. A large refractive index step means better optical confinement. Using the adaptive design [6], the waveguide thickness (d, *see* Fig. 2) is optimized in all scenarios to get the best possible confinement factor even with reduced refractive index step, *see* **Fig. 7**. Upon proper waveguide design [6], the maximum optical confinement factor attainable as a function of Sn composition is shown in **Fig. 7 (b)** for various QW thicknesses. For optimal waveguide design corresponding to the Sn composition, the $In_xGa_{1-x}As$ composition must be LM to $Ge_{1-y}Sn_y$, as discussed in **Fig. 4 (a)** and the thickness of the waveguide shown in **Fig. 7 (a)** must be selected. The thickness d shown in **Fig. 7 (a)** is the total optimal thickness of the $In_xGa_{1-x}As$ waveguide, *i.e.*, the $Ge_{1-y}Sn_y$ QW will be sandwiched between two $In_xGa_{1-x}As$ layers of thickness d/2. The thicknesses d/2 of the InGaAs waveguide are denoted in **Fig. 2 (b)**. **Figs. 7 (b)** and **(c)** summarize the design space while highlighting the interdependent impact of the QW thickness and Sn composition on the $Ge_{1-y}Sn_y$ SCH QW laser structure. A sample design point with a Sn composition of ~ 9 % and a QW thickness of 9 nm is marked in **Figs. 7(a)** and **(c)** as well as in **Fig. 1**. This $Ge_{1-y}Sn_y$ QW SCH structure will operate at ~ 2 µm wavelength and the cavity would have a confinement factor of 1.5 % provided the waveguide is designed at the optical cavity thickness of d = 300
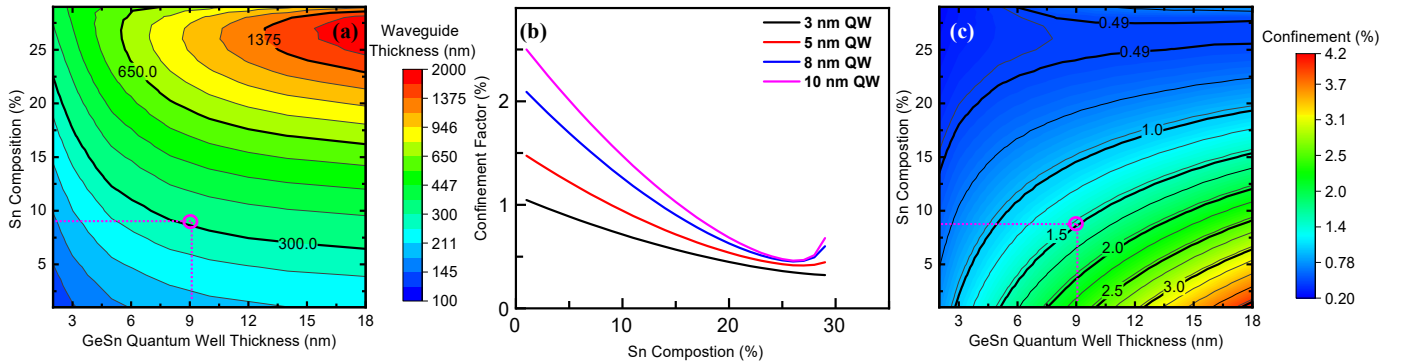

Fig. 7. $Ge_{1-y}Sn_y/In_xGa_{1-x}As$ LM SCH QW waveguide properties as a function of Sn composition: (a) optimum $In_xGa_{1-x}As$ waveguide thickness needed to achieve the optimum confinement factor when $In_xGa_{1-x}As$ and $Ge_{1-y}Sn_y$ are LM. (b) and (c) optimum confinement factor of the GeSn QW as a function of Sn composition and GeSn QW thickness. A specific design point is marked for discussion.

many optical modes for the E-field (TE as well as TM), this analysis only includes the fundamental TE and TM modes in the optical solver. The recombination from the HH band largely produces TE emissions, whereas the recombination from the LH band produces TM emissions, this is determined by the transition strengths in the GeSn QW [6, 32]. The actual mode

nm. At Sn compositions beyond 7-8 %, $Ge_{1-y}Sn_y$ transitions to a direct bandgap material and thus can provide relatively efficient lasing, making higher Sn compositions desirable. However, the Sn composition also affects the emission wavelength for the specific applications making the choice of Sn composition crucial.

E. Quantization effect and Sn alloying

An interdependent relationship exists between the impact of Sn alloying and the effect of quantization on the lasing operation of the $Ge_{1-y}Sn_y$ QW laser. It is interesting to note that due to the quantization of the energy levels in the $Ge_{1-y}Sn_y$ QW, the bandgap is not zero even at Sn = 25 %, contrary to the bulk $Ge_{1-y}Sn_y$ bandgap [27, 28]. This creates an exciting regime where the transition energy for the active region is largely determined by the quantization effect, with no or minimal contribution from the bulk bandgap. Increasing the Sn composition has the following effects on the $Ge_{1-y}Sn_y$ active region: (i) decreasing the effective mass of the Γ-valley [29], (ii) decreasing the effective mass of the LH-band [29] and (iii) lowering the Γ-valley. The decreasing effective mass results in a drastically large QC pushing the ground state eigen energy higher and consequently, the effective bandgap rises. Whereas, increasing Sn composition also decreases the bulk bandgap of $Ge_{1-y}Sn_y$ material. Thus, these two effects cause opposing impacts on the $Ge_{1-y}Sn_y$ emission characteristics. The rising ground state eigen energy at higher Sn compositions (a consequence of the lower effective mass) is shown in **Fig. 6**. A larger Sn composition produces a larger QC and Sn alloying impact on the lasing performance of the $Ge_{1-y}Sn_y$ QW laser. Thus, designing a $Ge_{1-y}Sn_y$ QW laser must include consideration of the Sn alloying effect on the bandgap as well as the Sn alloying effect on the effective mass and corresponding QC.

F. Material and Modal Gain for the GeSn QW laser

The material gain spectrum for the TE and TM mode emissions from the GeSn/InGaAs LM QW laser stack is shown in **Figs. 8 (a)** and **(b)**, respectively. Only the fundamental TE and TM modes are considered in the calculation for simplicity, in practice a quasi-TE and/or quasi-TM emission is expected as discussed earlier. Emissions are possible through the Γ-HH transition as well as Γ-LH transition [15, 16], and the relevant transitions in the energy range from 0.2 eV to 1 eV are considered and computed according to Fermi's Golden Rule [15, 16]. The TE mode gain dominates over the TM mode gain as the TE mode gain is produced mainly from the HH-band which has a higher DOS [6, 15]. The ground state transition Γ-HH is denoted by the "B" peaks shown in **Fig. 8 (a)**, and as the Sn composition is increased, the peak moves to a lower energy. Transitions from the LH band also contribute to the TE gain, but at a slightly higher emission energy due to the quantization-induced broken degeneracy of the LH and HH bands. These
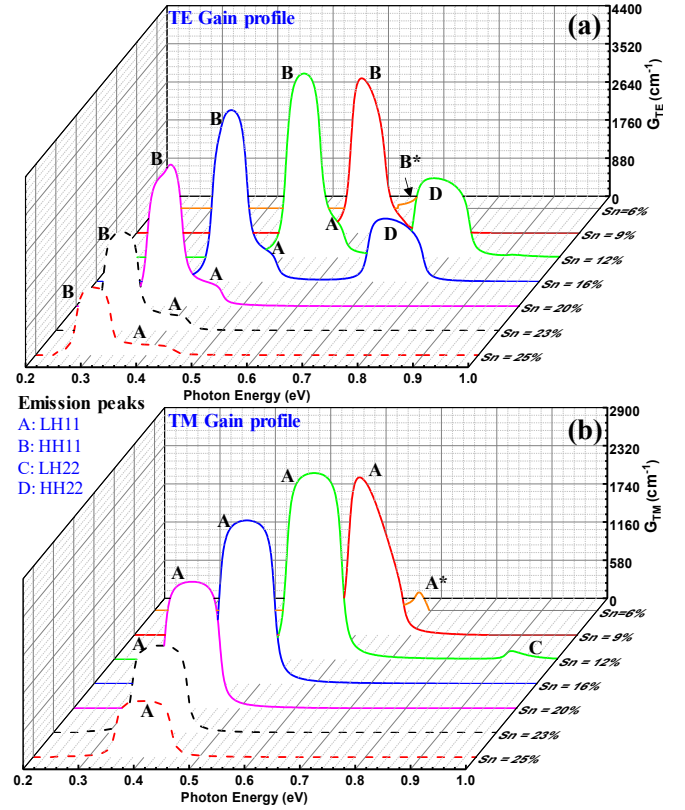
Fig. 8. Material Gain spectrum for a 10 nm GeSn QW for various Sn compositions at a maximum carrier injection level of ~ 10^{13} cm^{-2}: (a) TE mode gain and (b) TM mode gain. (*) a higher injection level compared to others is used to get some gain due to the insulating nature of the stack.

ground state Γ-LH transitions denoted by the peak labeled "A" are shown in **Fig. 8 (a)**. Emission from the second order transitions are possible at higher emission energies and higher excitation levels, and the peaks associated with the first excited state Γ-HH transition are shown in **Fig. 8 (a)** labeled as "D". Similarly, the TM mode gain is computed and shown in **Fig. 8 (b)**. The TM gain originates primarily from the ground state and excited state of the Γ-LH transitions [6, 15]. Note that a minute TE and TM gain peak is observed for the 6 % GeSn QW laser configurations in **Figs. 8 (a)** and **(b)**, respectively. For low Sn compositions, due to the poor conductivity of the surrounding InAlAs layers (very low In %), a sufficient quasi fermi-level separation for the GeSn/InGaAs/InAlAs laser stack cannot be achieved for realistic injection levels. Hence, the proposed GeSn/InGaAs/InAlAs SCH QW laser stack cannot function as

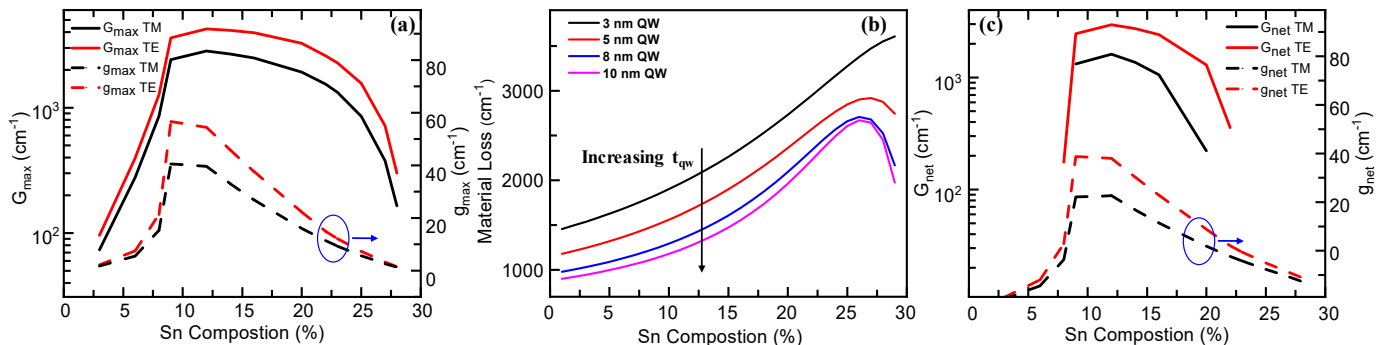Fig. 9. Lasing performance of the 10 nm GeSn QW as a function of Sn composition: (a) The maximum material and modal gain at a maximum carrier injection level of ~ 10^{13} cm^{-2}, (b) the loss associated with the laser cavity for various quantum well thicknesses, and (c) the net material and modal gain potentially achievable beyond losses at a maximum carrier injection level of ~ 10^{13} cm^{-2}.

an efficient laser at Sn compositions below 7 %, as is evident from the maximum gain shown in **Fig. 9**.

The maximum material and modal gain for the TE and TM modes are shown in **Fig. 9 (a)**. At the electrical probes (outside the *n* and *p* regions in Fig. 2), the bias is increased resulting in a modulation of the fermi levels in the hetero-stack and a corresponding increase in separation of the quasi-fermi levels in GeSn QW and a rise in injection carrier density. The gain nearly saturates at higher injection levels, this can be seen in **Fig. 10 (a)**, as well as in typical III-V lasers shown in Ref. [35]. This saturation value is the maximum gain shown here in **Fig. 9**. There exists an optimum range of Sn compositions between 8 - 18 %, where this GeSn QW laser stack can provide excellent material gain at realistic injection levels. At low Sn compositions below 7 %, the material gain is low due to the poor fermi-level modulation associated with the low conductivity high bandgap InAlAs layers in the stack as well as the poor directness of GeSn. As the Sn composition is increased, the DOS effective mass of the Γ-valley electrons reduces, while also reducing the joint-DOS in a nearly linear fashion and consequently reducing the gain factor [29]. According to Fermi's Golden rule, the transition rate for a constant photon density depends inversely on the transition energy [16], indicating that transitions that have a smaller energy difference would be more likely and will produce greater gain. Expectedly, as the Sn composition in the GeSn QW is increased, the effective transition energy reduces (*see*, **Fig. 5**), increasing the transition rate as well as the gain factor. The momentum matrix element that determines the polarization-specific transition strength also depends on the effective mass and the transition energies, thus affecting the Sn composition dependence of the gain in more subtle ways. Due to the opposing effect of the transition rate (increasing) and DOS (reducing) on the Sn-composition dependence of the material gain, there exists a brief range of Sn compositions between 8 - 18 % where the gain factor increases or remains nearly constant even though the DOS drops linearly. The maximum gain is further scaled by the fermi factor which generates the material gain seen in **Fig. 9 (a)**. Beyond a Sn composition of 16 – 18 %, the DOS reduction (due to reducing effective mass) dominates, resulting in a drastic drop in material gain. Finally, the dependence of the maximum material gain (*see*, **Fig. 9a**) on the Sn composition in the GeSn QW can be understood through 3 regions: (i) at low Sn compositions below 7 %, the gain factor is large and nearly constant but the fermi level modulation is not possible due to the AlAs in the SCH resulting in low gain, (ii) at Sn compositions between 8 – 18 %, the gain factor approaches a maximum value and remains nearly constant while the InAlAs SCH allows fermi level modulation and population inversion resulting in a maxima for the gain, and (iii) beyond ~ 18 %, the gain factor drops drastically due to low DOS resulting in a poor gain further degraded by the large separation between the bandgap and the effective bandgap due to QC. The modal gain is obtained by accounting for the confinement factor (**Fig. 7b** and **c**) for the GeSn QW and is shown in **Fig. 9 (a)**. It follows a similar trend to the material gain and a peak modal gain value of ~ 60 cm^{-1} can be attained near Sn ~ 14 % for an emission wavelength of 2.6 μm.

As the QW thickness is increased, a larger optical confinement factor can be attained due to a larger overlap with the emission field [6, 15]. On the other hand, as the Sn composition is increased, the emission wavelength increases, and the optical confinement factor reduces. These trends of the optical confinement factor are summarized in **Figs. 7 (b)** and **(c)** also affect the cavity losses as shown in **Fig. 9 (b)** [6]. These losses are calculated assuming a free carrier absorption of 500 cm^{-1} and a mirror loss of 10 cm^{-1}, similar to the GeSn values reported in Ref. 11. Based on the material gain and loss, the net material and modal gain (*gain - loss*) are determined as shown in **Fig. 9 (c)**. Eventually, at Sn ~ 22 % the net modal gain becomes < 0 indicating no net lasing. A significant TE net modal gain of ~ 40 cm^{-1} can be attained at Sn ~ 14 % for the GeSn proposed QW laser structure. Net material and modal gains approaching ~ 3000 cm^{-1} and 40 cm^{-1} indicate that the proposed GeSn QW laser stack is an interesting avenue to explore lasing from this material system.

G. Threshold current estimates for the GeSn QW laser

Sn alloying in GeSn produces a downward shift in the Γ-valley and has a low impact on the L-valley, unlike the tensile Ge QW case where the L-valley also descends with a certain rate [6]. This proves to be a significant advantage for the injection performance of the GeSn QW-based laser because, with rising Sn composition, the probability of occupation of the L-valley decreases much faster. Carriers in the L-valley do not participate in optical transitions due to the indirect nature of the transition, resulting in loss of carriers, high $J_{TH,}$ and poor IQE. As the L-valley has a large DOS, de-populating this valley is critical and non-trivial, alloying with Sn greatly reduces its occupancy enabling the GeSn QW laser to have low J_{TH}. Furthermore, as seen earlier, the joint-DOS reduces linearly with increasing Sn composition due to the effective mass. A smaller DOS in the QW enables transparency to be achieved at lower injection levels enabling a low J_{TH} provided there is some net gain. The J_{TH} is determined by the transparency injection level as well as the loss in the waveguide. Between 8 – 18 % Sn composition, the joint-DOS decreases linearly, but the material gain and the net gain remain high and non-decreasing (*see*, **Fig. 9(a)**). Hence, we can expect the GeSn QW laser to provide drastically low J_{TH} with a good net gain.

The current injection performance of the GeSn QW laser structure is summarized for Sn = 9, 12, and 16 % in **Fig. 10 (a)**. The gain characteristics move to lower current levels as the Sn composition is increased indicating that the transparency in the GeSn active layer is achieved at lower injection levels. Based on the total losses shown in **Fig. 9 (b)** and the material gain injection profile shown in **Fig. 10 (a)**, the J_{TH} can be determined as the injection current required to overcome the losses. This J_{TH} is shown in **Fig. 10 (b)** and an inflection point can be observed near Sn = 14 %, where the J_{TH} is the lowest. At large Sn compositions beyond ~ 20 %, the J_{TH} is large due to the high loss associated with the poor optical confinement as well as the reduced net gain. At low Sn compositions below Sn ~ 7 %, the J_{TH} is large due to the poor injection capability of the laser stack resulting in low fermi-level modulation, and low gain in the QW. At Sn ~ 14 %, the J_{TH} as low as ~ 10 A/cm^2 can be achieved for the TE mode owing to the cumulative additive effect of (i) QW configuration, (ii) large energy separation
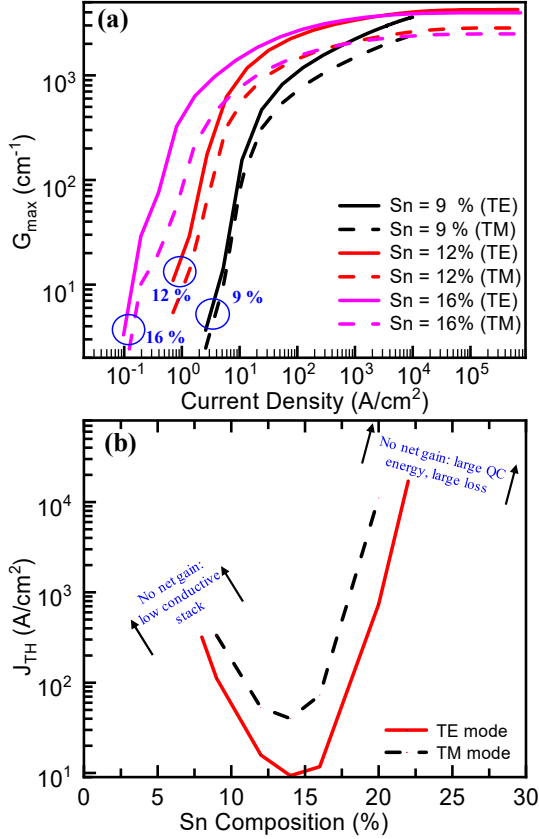
Fig. 10. (a) Material Gain as a function of current injection. (b) Threshold current density required to overcome losses as a function of Sn composition in a 10 nm GeSn QW laser stack.

active layers. The InAs composition in InGaAs required to create a small tensile strain of 1 % (t1), 2 % (t2) as well as a small compressive strain of 1 % (c1) and 2 % (c2) is shown with respect to the LM case, shown in **Fig. 11**, where InAs compositions for each compressive and tensile strained are indicated in this figure. A potentially additive effect of tensile strain and Sn alloying in the GeSn active layer could enable efficient lasing from group-IV-based materials. Furthermore, in the large-scale growth of these GeSn-InGaAs-InAlAs SCH structures, the LGB relaxation and design are crucial and challenging as pointed out earlier. Using the InAs composition as a tuning mechanism following **Fig. 11**, designers can offset unwanted strain in the LGB or material stack to ensure desired LM properties in the active region.
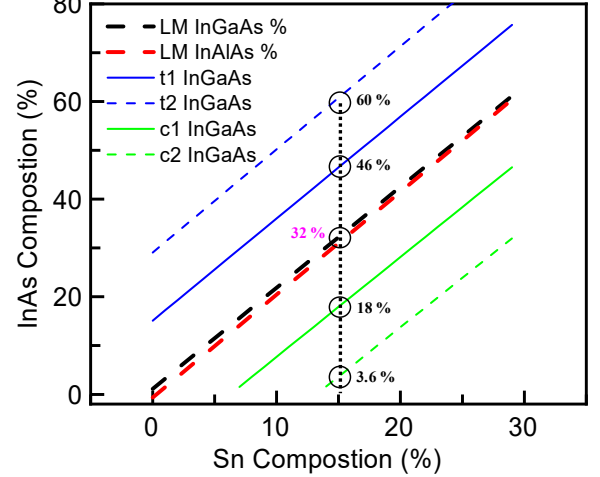

Fig. 11. An extension beyond LM GeSn QW: The proposed GeSn SCH QW system can also leverage the potential benefits of a small tensile or compressive epitaxial strain provided the benefits of strain outweigh the benefits of LM.

between the Γ- and L- valleys, (iii) strongly direct bandgap nature of GeSn at Sn = 14 %, (iv) low bandgap of GeSn, (v) sufficient band offsets, (vi) low joint-DOS, (vii) SCH optical confinement, (viii) low absorption losses, (ix) non-decreasing and high gain between Sn ~ 8 - 18 % although DOS decreases, and (x) reduced non-radiative recombination rates justified by the virtually defect-free LM interfaces.

H. Tensile and compressively strained GeSn QW designs

Considering the growing number of investigations in achieving lasing and improving the lasing performance of Ge, SiGeSn, and GeSn-based light sources, additional design flexibility for future modifications could be beneficial. Although the $Ge_{1-y}Sn_y$ QW design proposed here is a fully lattice matched system, various reports have studied light emission from Ge-based sources (theory as well as experiment) using epitaxial compressive [11] and tensile strain [4, 6, 36]. A detailed report on tensile strained Ge QW laser and lasing from Ge (and GeSn) based systems is summarized in Ref. 6. As the explorative efforts for GeSn lasers are still in the early stages of investigations, compressive strain in GeSn is also being investigated on Si or GaAs systems [12, 37 - 39]. Considering this evolving research area, compressive and tensile strain in $Ge_{1-y}Sn_y$ could prove to be technologically feasible as well as provide performance benefits. The $Ge_{1-y}Sn_y/In_xGa_{1-x}As$ SCH QW structure can be used to introduce a small mismatch, either compressive or tensile by changing the InAs composition in the structure away from LM. Such a system could be used to tune the lasing performance of single QWs, MQWs, and strain-balanced structures by creating tensile or compressive GeSn

I. GeSn-InGaAs MQW lattice matched laser

An interesting avenue for the proposed lattice matched system is utilizing the growth ease associated with the LM to form a GeSn-on-InGaAs-on-InAlAs MQW SCH laser structure with type I alignment. Such a system would provide similar advantages to the GaAs-AlGaAs material system which revolutionized semiconductor lasers over the last half century [15, 17, 36]. Although such a GeSn-InGaAs MQW material system has not been reported yet, it shows great promise due to the possibility of large gain, lower J_{TH}, low defects due to the LM, direct bandgap nature of GeSn and III-V epi-growth know-how as well as the accelerating GeSn popularity. Moving to a GeSn MQW system from a SQW laser stack, certain physical phenomena need to be considered. Here, we list and qualitatively discuss some of these effects. Certain defects and dislocations may be present in any real heteroepitaxial system, and a detailed characterization of these issues can help quantify and understand the impact of the defects. However, a lattice matched system is the best-known method to have the least defects in heteroepitaxial multilayer systems. In MQW systems, these potential defects may interact with each QW differently creating an unwanted impact on the gain, confinement, band alignment, offsets, and the injection into each QW. This can result in noise, reliability, and loss in lasing performance metrics such as gain and IQE. Additionally, incomplete relaxation of the underlying LGB can result in residual strain in the active region which can relax and create defects in the QW

regions which are inherently unpredictable. This can again adversely affect the lasing metrics such as IQE and loss.

The confinement factor is expected to increase with an increase in the number of QWs due to a larger overlap with the optical field and a larger emitting volume [15, 17]. There is an initial increase due to a larger geometrical overlap, this eventually saturates [15, 36]. There will be an optimum number of QWs for maximum confinement factor and this will depend on the wavelength, QW thickness, composition, and SCH waveguide stack [36]. Beyond this optimum number, the J_{TH} will rise significantly without providing a gain benefit. Each QW active region will not overlap the same with the optical field, so the contribution of gain from each QW will be different. For a symmetric design, the central QW could be aligned perfectly with the E-field peak resulting in a maximum contribution to the confinement factor and the gain. The QWs toward the edges will have a smaller E-field overlap resulting in a smaller confinement factor and a smaller gain. For every additional GeSn QW, a non-emitting InGaAs QW barrier is also added, and since the confinement factor has a large geometrical dependence, these increasing barrier layers result in reducing confinement factor.

The modal gain is expected to rise linearly with the number of QWs following the confinement factor trend (material gain remains nearly independent of the number of QWs). The threshold current density (and J_{MAX}) will increase linearly with the number of QWs due to a larger number of carriers that are now required in the active regions, owing to the increased volume of the active region. Although many QWs can provide a large gain, this comes at the cost of higher current consumption through the J_{TH} [40] and J_{MAX}. IQE is an intrinsic material property dependent on the band structure of GeSn QW and defects and various transitions in the active QW, it would not be affected by many QWs. Considering these factors, certain ideal-case estimates can be predicted for a 3 QW GeSn-InGaAs lattice matched laser. The Sn and In composition can be assumed to be 15 % and 30 %, respectively, resulting in an emission of 2.7 μm. Upon optimizing the waveguide cavity based on the adaptive design, one can expect an optical confinement factor of nearly 3 % (~ 3× with respect to **Fig. 7b**) and material gain of ~ 4000 cm^{-1} (*see* **Fig. 9a**) with a material loss of ~1500 cm^{-1} (*see* **Fig. 9b**). The net modal gain in this 3 QW system can be estimated to be 75 cm^{-1} with a J_{TH} of ~ 30 A/cm^2.

V. Conclusion

Through this work, a GeSn QW SCH architecture and the corresponding design methodology are proposed which can ensure lattice matching in the entire laser stack while providing desirable properties for efficient lasing. These desirable properties include good band offsets for room temperature operation, virtually defect-free stack and interfaces, monolithic structure, good net gain, low J_{TH}, and tunable operation. The GeSn/InGaAs/InAlAs system provides a SCH structure suitable for confining the optical field in the waveguide as well as carriers in the QW. The optimum cavity design through the adaptive design methodology is discussed to maximize the optical confinement of the field and its composition dependence for the GeSn QW SCH is discussed. The growth of such a material stack through MBE as well as the key design metrics

associated with the LGB are discussed. Using the TCAD simulator and custom gain solver, the optical gain spectrum is estimated as a function of Sn composition in the GeSn QW. A net material and modal gain of ~ 3000 cm^{-1} and ~ 40 cm^{-1}, respectively, can be achieved upon optimal cavity design for a Sn composition of 14 % at an emission wavelength of 2.6 μm. The optimum J_{TH} and net gain can be achieved for the GeSn SCH laser structure in the Sn compositions range between 8 - 18 %. This optimum J_{TH} and the high net gain are possible due to the improved Γ-L separation, low joint-DOS with a non-decreasing gain factor, low absorption, and carrier losses associated with the LM interfaces. This LM GeSn SCH QW laser structure has the potential to be an efficient, reliable, and tunable (1.2 μm to 6 μm wavelength) room temperature light source, which can be monolithically integrated on a GaAs substrate. Lastly, deviating from LM to achieve compressive or tensile strain in GeSn may prove useful in certain applications that can tolerate some defects and potentially benefit from strain. By carefully controlling the InAs composition in the proposed laser stack, specific amounts of tensile or compressive strains can be achieved in the proposed laser structure or unwanted strain can be compensated. Utilizing this approach, one could envision a tensile strained GeSn active layer for efficient lasing, which could potentially benefit from the additive effect of tensile strain along with Sn alloying in GeSn-based light sources.

VI. References

[1] W. Rachmady et al., "300mm Heterogeneous 3D Integration of Record Performance Layer Transfer Germanium PMOS with Silicon NMOS for Low Power High Performance Logic Applications," *IEEE IEDM Tech. Dig.*, Dec. 2019, pp. 29.7.1-29.7.4, doi:10.1109/IEDM19573.2019.8993626.

[2] R. Joshi, S. Karthikeyan and M. K. Hudait, "Monolithically Cointegrated Tensile Strained Germanium and InxGa1-xAs FinFETs for Tunable CMOS Logic," *IEEE Trans. on Electron Dev.*, vol. 69, no. 8, pp. 4175-4182, Aug. 2022, doi: 10.1109/TED.2022.3181112.

[3] R. Joshi, S. Karthikeyan and M. K. Hudait, "Germanium Nanosheet-FETs Scaled to Subnanometer Node Utilizing Monolithically Integrated Lattice Matched Ge/AlAs and Strained Ge/InGaAs," *IEEE Trans. on Electron Dev*, vol. 70, no. 3, pp. 899-907, March 2023, doi: 10.1109/TED.2023.3238376.

[4] M. K. Hudait, *et al.*, "Design, Theoretical, and Experimental Investigation of Tensile-Strained Germanium Quantum-Well Laser Structure", *ACS Appl. Electron. Mater.*, 3, 10, 4535–4547, 2021, doi: 10.1021/acsaelm.1c00660.

[5] K. Tani, T. Okumura, K. Oda, M. Deura, and T. Ido, "On-chip optical interconnection using integrated germanium light emitters and photodetectors," *Opt. Express*, vol. 29, no. 18, pp. 28021-28036, Aug. 2021, doi: 10.1364/OE.432324.

[6] R. Joshi, S. Johnston, S. Karthikeyan, L. F. Lester and M. K. Hudait, "Monolithically Integrated ε -Ge/InxGa1-xAs Quantum Well Laser Design: Experimental and Theoretical Investigation," *IEEE J. of Sel. Topics in Quantum Electronics*, doi: 10.1109/JSTQE.2023.3323336.

[7] Y. Cai *et al.*, "Analysis of Threshold Current Behavior for Bulk and Quantum-Well Germanium Laser Structures," *IEEE J. of Sel. Topics in Quantum Electronics*, vol. 19, no. 4, pp. 1901009-1901009, July-Aug. 2013, Art no. 1901009, doi: 10.1109/JSTQE.2013.2247573.

[8] H. Mahmudlu, *et al.*, "Fully on-chip photonic turnkey quantum source for entangled qubit/qudit state generation", *Nat. Photon.*, 2023, doi:10.1038/s41566-023-01193-1.

[9] R. E. Camacho-Aguilera, *et. al*, "An electrically pumped germanium laser," *Opt. Express 20*, 11316-11320, 2012, doi:10.1364/OE.20.011316.

[10] A. Ghosh, *et al.*, "Growth structural and electrical properties of germanium-on-silicon heterostructure by molecular beam epitaxy", *AIP Adv.*, vol. 7, no. 9, Sep. 2017, doi: 10.1063/1.4993446.

[11] Wirths, S., *et al.*, "Lasing in direct-bandgap GeSn alloy grown on Si" *Nature Photon* 9, 88–92, 2015 doi: 10.1038/nphoton.2014.321.

[12] Yiyin Zhou, *et. al.*, "Electrically injected GeSn lasers with peak wavelength up to 2.7 μm," *Photon. Res.* 10, 222-229 (2022).

[13] M. K. Hudait, *et al.*, "High carrier lifetimes in epitaxial germanium-tin/ Al(In)As heterostructures with variable tin composition", *J. of Mat. Chemistry C* 10: 10530-10540 (2022). doi: 10.1039/D2TC00830K.

[14] D. Sukhdeo, *et. al.*, "Impact of minority carrier lifetime on the performance of strained germanium light sources", *Optics Comm*, Vol. 364, pp 233-237, April 2016, doi: 10.1016/j.optcom.2015.11.060.

[15] L. A. Coldren, S. W. Corzine, M. L. Mašanović, Diode Lasers and Photonic Integrated Circuits, John Wiley & Sons, 2012.

[16] S. L. Chuang, Physics of Photonic Devices, Second Edition, John Wiley & Sons, 2009.

[17] Y. Arakawa and A. Yariv, "Theory of gain, modulation response, and spectral linewidth in AlGaAs quantum well lasers," *IEEE J. of Quantum Electronics*, vol. 21, no. 10, pp. 1666-1674, Oct 1985, doi: 10.1109/JQE.1985.1072555.

[18] R. People and J. C. Bean, "Calculation of critical layer thickness versus lattice mismatch for Ge_xSi_{1-x} /Si strained-layer heterostructures," *Appl. Phys. Lett.*, vol. 47, no. 3, pp. 322–324, Aug. 1985. doi: 10.1063/1.96206

[19] G. -E. Chang, S. -W. Chang and S. L. Chuang, "Strain-Balanced Ge_zSn_{1-z}--$Si_xGe_ySn_{1-x-y}$ Multiple-Quantum-Well Lasers," *IEEE J. of Quantum Electronics*, vol. 46, no. 12, pp. 1813-1820, Dec. 2010, doi: 10.1109/JQE.2010.2059000.

[20] D. J. Richardson, "Filling the light pipe", *Science* 330, 327–328, 2010, doi: 10.1126/science.1191708.

[21] X. J. Yang, A. Li, R. Glaser, and J. X. Zhong, "The C-H stretching features at 3.2-3.5 μm of polycyclic aromatic hydrocarbons with aliphatic side groups" *The Astrophysical Journal*, **825** (1), 22 (2016). doi:10.3847/0004-637X/825/1/22

[22] S.-K. Liao, et al., "Long-distance free-space quantum key distribution in daylight towards inter-satellite communication", *Nat. Photonics* 11, 509–513, 2017, doi: 10.1038/nphoton.2017.116.

[23] G. L. Mansell, et al., "Observation of squeezed light in the 2 μm region", *Phys. Rev. Lett.* 120, 203603, 2018, doi: 10.1103/PhysRevLett.120.203603.

[24] Mancinelli, M, et al., "Mid-infrared coincidence measurements on twin photons at room temperature", *Nat Comm*., 8, 15184, 2017, doi:10.1038/ncomms15184.

[25] Høgstedt, L. et al., "Low-noise mid-IR upconversion detector for improved IR-degenerate four-wave mixing gas sensing", *Opt. Lett.* 39, 5321–5324, 2014, doi: 10.1364/OL.39.005321.

[26] S. Karthikeyan, *et. al*, "Lattice matched GeSn/InAlAs heterostructure: Role of Sn in energy band alignment, atomic layer diffusion and photoluminescence", *Journal of Mat. Chemistry C*, 11: 9472-9485 (2023). 10.1039/D3TC01018J

[27] J. I. Chyi, J. L. Shieh, J. W. Pan, and R. M. Lin, "Material properties of compositional graded $In_xGa_{1-x}As$ and $In_xAl_{1-x}As$ epilayers grown on GaAs substrates", *J. Appl. Phys*., 79 (11), 8367-8370, 1996, doi: 10.1063/1.362555

[28] Suyog Gupta, *et al*, "Highly Selective Dry Etching of Germanium over Germanium–Tin ($Ge_{1-x}Sn_x$): A Novel Route for $Ge_{1-x}Sn_x$ Nanostructure Fabrication" *Nano Letters* 2013 13 (8), 3783-3790 doi: 10.1021/nl4017286

[29] Zhigang Song, *et al*, "Band structure of $Ge_{1-x}Sn_x$ alloy: a full-zone 30-band k · p model", *New J. Phys*. 21, 2019, 073037, doi: 10.1088/1367-2630/ab306f.

[30] V. Swaminathan and A. T. MacRander, in Materials Aspects of GaAs and InP Based Structures, Prentice Hall, Englewood Cliffs, NJ, U.S., 1991.

[31] TCAD Sentaurus Device Manual Release: T-2022.03, Synopsys Inc., Mountain View, CA, USA, 2022.

[32] S. -W. Chang and S. L. Chuang, "Theory of Optical Gain of Ge--$Si_xGe_ySn_{1-x-y}$ Quantum-Well Lasers," *IEEE J. of Quantum Electronics*, vol. 43, no. 3, pp. 249-256, March 2007, doi: 10.1109/JQE.2006.890401.

[33] J. Liu, *et. al*., "Tensile-strained, n-type Ge as a gain medium for monolithic laser integration on Si," *Opt. Express* 15, 2007, 11272-11277, doi: 10.1364/OE.15.011272.

[34] M. K. Hudait, Y. Zhu, N. Jain, and J. L. Hunter, Jr., "Structural, morphological, and band alignment properties of GaAs/Ge/GaAs heterostructures on (100), (110) and (111)A GaAs substrates", *J. Vacuum Science & Technology B* 31: 011206, 2013, doi: 10.1116/1.4770070.

[35] M. Asada, A. Kameyama and Y. Suematsu, "Gain and intervalence band absorption in quantum-well lasers," *IEEE Journal of Quantum Electronics*, vol. 20, no. 7, pp. 745-753, July 1984, doi: 10.1109/JQE.1984.1072464.

[36] Quang Minh Thai, *et al*, "GeSn optical gain and lasing characteristics modelling" *Phys. Rev. B* 102, 155203 doi:10.1103/PhysRevB.102.155203

[37] Calbi Gunder *et. al*, "The growth of Ge and direct bandgap $Ge_{1-x}Sn_x$ on GaAs (001) by molecular beam epitaxy", *RSC Adv.*, 2024, 14, 1250, doi: 10.1039/d3ra06774b.

[38] Dou, W. (2018). High-Sn-content GeSn Alloy towards Room-temperature Mid Infrared Laser. Graduate Theses and Dissertations Retrieved from https://scholarworks.uark.edu/etd/2849.

[39] Bahareh Marzban *et al*, "Strain Engineered Electrically Pumped SiGeSn Microring Lasers on Si", *ACS Photonics* 2023, 10, 1, 217–224, doi: 10.1021/acsphotonics.2c01508.

[40] A. Sugimura, "Threshold currents for AlGaAs quantum well lasers," in IEEE Journal of Quantum Electronics, vol. 20, no. 4, pp. 336-343, April 1984, doi: 10.1109/JQE.1984.1072405

Rutwik Joshi (Student Member, IEEE) received his Master's of Technology degree specializing in Microelectronics from the Indian Institute of Technology, Delhi, India, in 2019. He is currently working towards his Ph.D. degree in the Department of Electrical and Computer Engineering at Virginia Polytechnic Institute and State University, USA. He is a part of the ADSEL Group at Virginia Tech working on material and device research exploring Ge-based nanoscale quantum well lasers and transistors. Before joining Virginia Tech, he worked as an AMS engineer at Intel Corp specializing in device/circuit reliability CAD and EM/IR.

Mantu K. Hudait (M'08, SM'08) received an M.S. degree in materials science and engineering from IIT Kharagpur, Kharagpur, India, and a Ph.D. degree in materials science and engineering from Indian Institute of Science, Bangalore, India, in 1999. From 2000 to 2005, he was a Postdoctoral Researcher at Ohio State University and worked on the mixed cation and mixed anion metamorphic buffer, low bandgap thermophotovoltaics, and heterogeneous integration of III-V solar cells on Si. From 2005 to 2009, he was a Senior Engineer in the Advanced Transistor and Nanotechnology Group at Intel Corporation. In 2009, he joined the Bradley Department of Electrical and Computer Engineering at Virginia Tech as an Associate Professor. He has over 205 technical publications and refereed conference proceedings and holds 60 US patents. His current research at Virginia Tech focuses on the heterogeneous integration of compound semiconductors and GeSn on Si for photonics, quantum-well transistors, and photovoltaics. His research interests include III-V compound semiconductor epitaxy, metamorphic buffer, mixed As-Sb, and mixed As-P-based devices. He has received two Divisional Recognition Awards from Intel Corporation.

Luke F. Lester, an IEEE and SPIE Fellow, joined Virginia Tech in 2013 as the Head of the Bradley Department of Electrical and Computer Engineering (ECE) and was named the Roanoke Electric Steel Professor in 2016. Prior to joining VT, he was a professor of ECE at the University of New Mexico (UNM) from 1994 to 2013. Before joining UNM, Dr. Lester worked as an engineer for the General Electric Electronics Laboratory in Syracuse, New York for 6 years where he co-invented the first Pseudomorphic HEMT, a device that was later highlighted in the Guinness Book of World Records as the fastest transistor. Later as a PhD student at Cornell, he researched and developed the first strained quantum well lasers that are now the industry standard for optical transmitters in data and telecommunications links. In 2001, he was a co-

founder and Chief Technology Officer of Zia Laser, Inc., a startup company using quantum dot laser technology to develop products for communications and computer/microprocessor applications. The company was later acquired by Innolume, GmbH. In 2012 he received the Harold E. Edgerton Award of the SPIE for his pioneering work on ultrafast quantum dot mode-locked lasers. He has published 148 journal articles and some 260 other publications. He was Editor-in-Chief of the IEEE Journal of Selected Topics in Quantum Electronics for 3 years from 2015-17.